Towards General Purpose Vision Foundation Models for Medical Image Analysis: An Experimental Study of DINOv2 on Radiology Benchmarks

Anonymous authors
Paper under double-blind review

Abstract

The integration of deep learning systems into healthcare has been hindered by the resource-intensive process of data annotation and the inability of these systems to generalize to different data distributions. Foundation models, which are models pre-trained on large datasets, have emerged as a solution to reduce reliance on annotated data and enhance model generalizability and robustness. DINOv2 is an open-source foundation model pre-trained with self-supervised learning on 142 million curated natural images that exhibits promising capabilities across various vision tasks. Nevertheless, a critical question remains unanswered regarding DINOv2's adaptability to radiological imaging, and whether its features are sufficiently general to benefit radiology image analysis. Therefore, this study comprehensively evaluates the performance DINOv2 for radiology, conducting over 200 experiments across diverse modalities (X-ray, CT, and MRI). To measure the effectiveness and generalizability of DINOv2's feature representations, we analyze the model across medical image analysis tasks including disease classification and organ segmentation on both 2D and 3D images, and under different settings like kNN, few-shot learning, linear-probing, end-to-end fine-tuning, and parameter-efficient fine-tuning. Comparative analyses with established supervised, self-supervised, and weakly-supervised models reveal DINOv2's superior performance and cross-task generalizability. The findings contribute insights to potential avenues for optimizing pre-training strategies for medical imaging and enhancing the broader understanding of DINOv2's role in bridging the gap between natural and radiological image analysis.

1 Introduction

Radiology imaging plays a pivotal role in modern medicine, serving as an indispensable tool for accurate and timely diagnosis (Hussain et al., 2022). The importance of radiological imaging lies in its ability to provide detailed and non-invasive visualizations (Peng et al., 2022) of the internal structures and functions of the human body. Deep learning-based computer vision methods have been successful at analyzing and processing radiological imaging, leading to systems that can extract clinically-relevant information with high accuracy (Rajpurkar et al., 2017). However, the success of these systems has been reliant on annotated medical data, which is expensive to obtain because it requires the time and effort of trained radiologists (Khan et al., 2023). Moreover, these systems can achieve high-level accuracy only within a specified scope, but fail to generalize across domains, tasks, and slight data distribution shifts (Kelly et al., 2019).

Recently, the field of computer vision has seen a rise in interest for general-purpose models that are optimized to function across different tasks and domains (Yuan et al., 2021; Radford et al., 2021; Oquab et al., 2023; Kirillov et al., 2023). These models, grouped under the term "Foundation Models" (FMs), usually contain parameters ranging from hundreds of millions to tens of billions and are trained on large datasets, on the order of tens of millions. As a result of this large-scale training, these FMs often achieve state-of-the-art (SoTA)

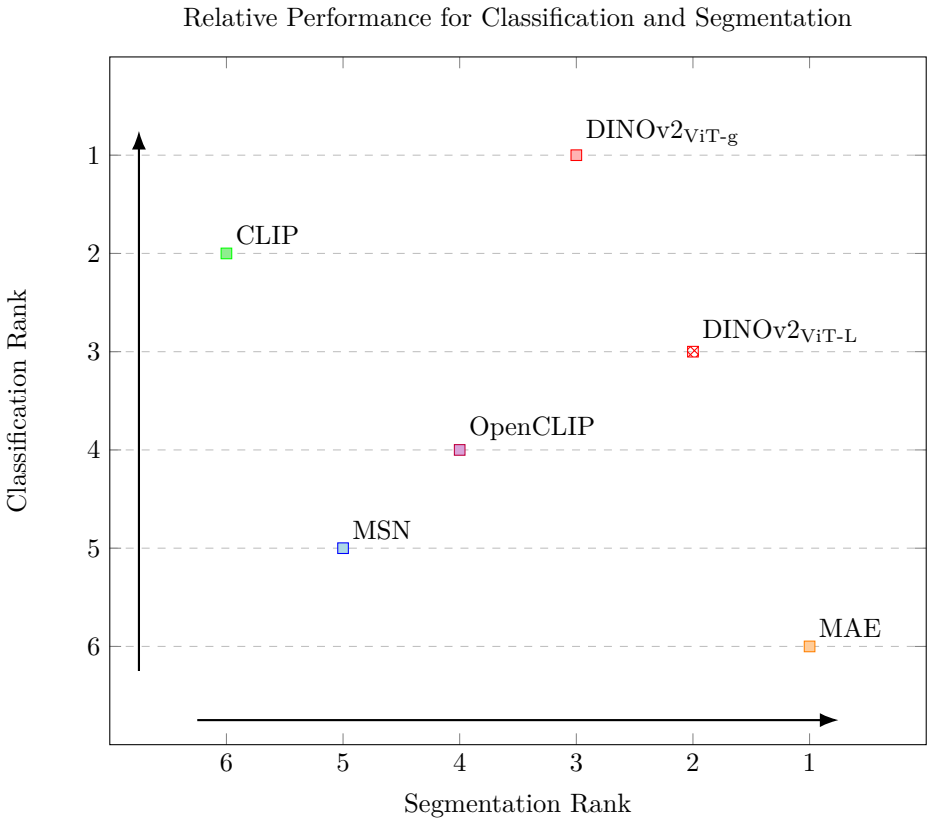

Figure 1: Cross-task generalizability of DINOv2 compared to other models. The horizontal axis shows the relative performance or ranking of each of the models on segmentation tasks, while the vertical axis does the same for classification tasks. The ranking is calculated as the average ranking across all segmentation (5 Datasets) or classification tasks (4 Datasets), where rank 1 means the model performs the best relative to other models. Models pre-trained with weakly-supervised learning perform well only on classification tasks, while MAE performs well only on segmentation. DINOv2 can generalize across both tasks and outperforms all other models for classification.

results and impressive zero-shot and few-shot performance and generalizability (Oquab et al., 2023; Kirillov et al., 2023). For these reasons, foundation models have gained traction in deep learning-based medical image analysis research (Zhou et al., 2023; Wang et al., 2023; Caro et al., 2023; Qiu et al., 2023; Ma et al., 2023), as they hold promise for reducing the reliance on the expensive process of annotating medical data and towards the goal of building generalist medical artificial intelligence systems that can function across a variety of tasks and domains (Moor et al., 2023).

1.1 What Are Foundation Models?

The term “Foundation Model" encompasses a broad spectrum of models that may initially appear distinct. In the most general sense, foundation models are large models trained on large datasets and can generalize across tasks and/or domains (Merritt, 2023). To make the term more useful in our analysis, we categorize foundation models using two distinct methods. First, we divide FMs depending on their training paradigm into three groups: self-supervised, weakly-supervised, and supervised foundation models. Weakly-supervised and supervised foundation models require correspondence in the training data. In these paradigms, the training data is required to be available in pairs: an X-ray examination and a corresponding interpretation, diagnosis, or segmentation mask for example. Models

like OpenAI's CLIP (Radford et al., 2021) and Meta's Segment Anything Model (SAM) (Kirillov et al., 2023) fall under this category. Self-supervised foundation models, on the other hand, require one input data to train (an image, text, audio, etc.) Meta's DINOv2 (Oquab et al., 2023) and Google's Universal Speech Model (USM) (Zhang et al., 2023) belong to this category.

Additionally, we categorize FMs into two groups depending on the generalizability of their produced representations: general purpose (also called task-agnostic), and task-specific FMs. General purpose foundation models produce features that generalize across more than one task, segmentation and classification for example, while task-specific models specialize on only one task. DINOv2 (Oquab et al., 2023) and USM (Zhang et al., 2023) fall under the former category while SAM (Kirillov et al., 2023) is under the latter.

Because of the less restrictive training dependencies for self-supervised FMs, we believe that they are a promising option to explore for future research especially for the medical imaging domain, since the shortage of training data is one of the main constraints for applications in the field (Khan et al., 2023). Reducing the requirement for annotated data significantly increases the set of possible data used for training, and using unannotated data makes it possible to combine data that are paired with different labels (for example, combining those with class labels and those with segmentation masks). Moreover, FMs that produce representations that can be used across a variety of tasks are desired because it is usually a signal of model robustness. As a result, we focus our attention on self-supervised general-purpose FMs for medical image analysis. Specifically, we adopt Meta's DINOv2 (Oquab et al., 2023) model, a publicly available general-purpose vision foundation model that can extract robust representations across different vision tasks, for experimentation on a wide range of medical disease classification and organ segmentation benchmarks, across different radiological exams and under different evaluation settings.

1.2 What is DINOv2?

DINOv2 is a successor of DINO (Caron et al., 2021) and constitutes both a self-supervised pre-training method based on DINO and iBOT (Zhou et al., 2022), and a collection of models pre-trained using that method. It was released to the public by Meta in April 2023 and promises robust representations that enable general-purpose functionality with visual-only data (Oquab et al., 2023). The released models were pre-trained on a dataset of 142 million carefully curated natural images, called LVD-142M. Roughly 100 million of these are images that are similar to ImageNet, curated from calculating similarly of web-scarpered images with ImageNet21k dataset (Deng et al., 2009). The remaining images were retrieved based on their similarity to Caltech 101 (Fei-Fei et al., 2004), ADE20k (Zhou et al., 2017), and Google Landmarks v2 (Weyand et al., 2020), among others. The models achieve competitive performance on classification, segmentation, depth estimation, and image retrieval tasks across both image and video benchmarks. Moreover, because of the adopted discriminative self-distillation approach, DINOv2 performs well "out-of-the-box" without the need to fine-tune the encoder. The giant version of the model (ViT-g/14) achieves an accuracy of 86.5% and 83.5% on Linear-probing and kNN evaluations, respectively, on ImageNet-1k, outperforming other weakly-supervised and self-supervised methods. This capability to perform well out-of-the-box is appealing, especially in the medical domain, as it implies competitive performance even in low-data and low-computation settings.

1.3 Contribution

In this paper, we set to work towards vision-only general-purpose foundation models for the medical domain by adopting DINOv2 for disease classification and organ segmentation benchmarks. We perform comprehensive evaluations of DINOv2 across various scenarios for multiple radiology modalities, exploring both low (few-shot) and high data settings spanning X-ray, CT, and MRI examinations. We benchmark DINOv2's performance with

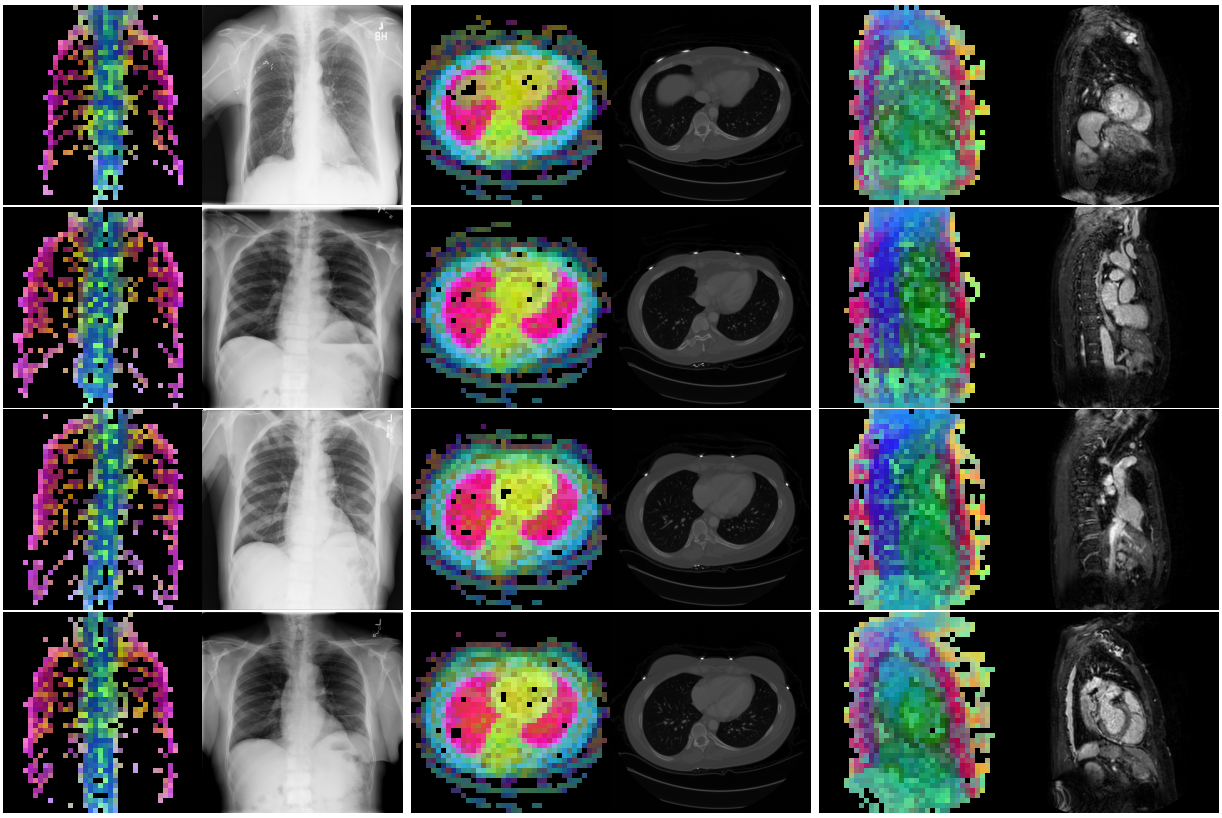

Figure 2: **PCA component visualization.** Following Oquab et al. (2023), the PCA is computed between patches of scans that are in the same column, and the first 3 components are shown. Thresholding is used on the first component to remove the background. Just like in natural images [8], the colors of the three PCA components correspond well with the same parts of images in the same category. This is an easier task however, compared to natural images, because there is less variability between examinations on medical images compared to natural images.

other natural-image supervised, self-supervised, and weakly-supervised models like CLIP, OpenCLIP, and SAM, among others shown in Table 2.

We evaluate DINOv2 on both disease classification and organ segmentation benchmarks. For disease classification tasks, we evaluate the model on kNN, linear-probing, few-shot learning, parameter-efficient fine-tuning, and end-to-end fine-tuning scenarios. For organ segmentation tasks we compare lightweight and non-lightweight decoders, while we keep the DINOv2 backbone frozen. We compared the results to supervised, weakly-supervised, and self-supervised models. As far as we know, there is no comprehensive analysis of DINOv2 on medical benchmarks that evaluates the model across disease classification and organ segmentation tasks and on different radiological examinations. Our contributions can be summarized as follows:

- Evaluate DINOv2 on disease classification and organ segmentation radiology benchmarks, under different evaluation settings. We conclude that DINOv2 outperforms self-supervised and weakly-supervised models on classification tasks and is competitive with supervised models pre-trained on ImageNet21K. For segmentation tasks, we observe that DINOv2 outperforms weakly-supervised methods by a large margin, and outperforms or is competitive with supervised methods trained end-to-end.
- Analyze the cross-task generalizability of DINOv2 compared to supervised, self-supervised, and weakly-supervised models. Our analysis concludes that weakly-

supervised models perform well on classification tasks only, and masked imaged modeling self-supervision performs well only on segmentation tasks, while DINOv2 can generalize across both tasks. DINOv2 also outperforms supervised classification models when evaluated on segmentation tasks, and outperforms SAM for disease classification.

- Employ parameter-efficient fine-tuning with a DINOv2 ViT-g/14 model on large X-ray classification datasets and provide a performance and efficiency comparison of PEFT with end-to-end fine-tuning and linear-probing. We conclude that using PEFT can yield performance that is competitive with end-to-end fine-tuning using less than 1% of the total model parameters.

2 Related Works

Supervised foundation models. Training a large-scale network with supervised learning is non-trivial because it is difficult to combine different labels together. This is even more true in the medical domain where labeled data is scarce. Even still when labels are seemingly similar, other issues can arise. Cohen et al. (2020) have attempted to train a large-scale X-ray foundation model with supervised learning by combining public chest X-ray disease classification datasets that share diseases. their analysis highlights the fact that discrepancies in labeling caused by disease concept shift across hospitals and observers can lead to worse generalizations for deep learning models.

Regardless, there successful attempts at building a large-scale supervised foundation model. The Segment Anything Model (SAM) (Kirillov et al., 2023), a supervised foundation model for prompt-based segmentation trained with automatically extracted segmentation masks, is one of those attempts. Since the release of SAM, its applicability for the medical images has been explored (He et al., 2023; Zhang & Jiao, 2023; Mazurowski et al., 2023). It's performance for medical segmentation was found to be inadequate in most cases and highly variable. Because of that, Ma et al. (2023) have developed MedSAM by adopting SAM for the medical domain using a dataset of more than one million medical images across diverse segmentation tasks and examination modalities. MedSAM significantly outperforms SAM on medical tasks and achieves comparable performance to U-Net (Ronneberger et al., 2015) models. Still, MedSAM is limited to medical segmentation, and it is unclear whether it can be generalized to other medical image analysis tasks.

Weakly-supervised foundation models. Previous research has explored weakly-supervised vision-language models for zero-shot classification, visual question answering, and image generation in the medical domain, achieving SoTA or competitive performance on radiology benchmarks (Wang et al., 2022; Chambon et al., 2022b; Zhang et al., 2022; Chambon et al., 2022a). Zhang et al. (2022) applied contrastive learning to paired X-ray image-report for learning visual representations. However, the availability of corresponding image-text pairs is a stringent requirement to be applicable for most medical datasets. Moreover, as highlighted by Wang et al. (2022), a false negative issue exists when applying this learning paradigm in the medical domain because, unlike diverse natural images, medical reports can describe other patients that are not necessarily paired. Instead, Wang et al. (2022) proposed MedCLIP, employing an extension of CLIP's contrastive pre-training method that utilizes unpaired examination-report samples, using the MIMIC-CXR (Johnson et al., 2019) and CheXpert (Irvin et al., 2019) datasets. They outperform previous SoTA on zero-shot and supervised classification on four radiology benchmarks. Yet, the performance of MedCLIP, along with other vision-language models, is still limited by the availability of text-image data.

Self-supervised foundation models. Self-supervised pre-training applied to medical datasets has recently achieved SoTA on CT and MRI segmentation benchmarks (Valanarasu et al., 2023; Tang et al., 2022). For example, Tang et al. (2022) pre-trained a Swin UNETR (Hatamizadeh et al., 2022) architecture with self-supervision on 5,050 CT volumes

and outperformed previous SoTA on the BTCV (Landman et al., 2015) and MSD (Antonelli et al., 2022) competitions. However, to the best of our knowledge, there is still no self-supervised general-purpose FM for the medical domain that has achieved consistently competitive results across tasks and radiological examinations.

3 Methodology

In this section, we describe the motivation for adopting DINOv2 for this study and outline the settings under which we performed our experiments. All the details about the pre-processing and hyperparameter tuning pipeline are publicly available in our code (available in Section 6).

3.1 Motivation for Using DINOv2

There are many vision foundation models trained with supervised, self-supervised, and weakly-supervised learning on natural images (Radford et al., 2021; Kirillov et al., 2023; Yuan et al., 2021; Xiao et al., 2023; Ilharco et al., 2021). However, we decided to employ DINOv2 in our analysis because of the robustness of its representations, achieving competitive performance in multiple downstream tasks, across vision modalities (image and video), and, most importantly, in out-of-the-box evaluations. The DINOv2 training paradigm was specifically designed to generate powerful representations on out-of-the-box kNN evaluations and outperforms many other weakly-supervised and self-supervised foundation models in kNN and linear-probing (Oquab et al., 2023).

3.2 Datasets

We evaluated DINOv2 on 9 public radiology benchmarks, spanning X-ray, CT, and MRI examinations (Exam.) for disease classification (CLS, 4 datasets) and organ segmentation (SEG, 5 datasets) tasks. A summary of the used datasets is shown in Table 1. “# Classes" describes the number of classes and “# Images/Volumes" describes the number of images for 2D datasets and volumes for 3D datasets, respectively. They describe the number of images or volumes that we use for each dataset, and not the number in the original dataset. This is because some of the datasets used have subsets that are not publicly accessible, like the test sets in MSD (Antonelli et al., 2022). Moreover, we only used a subset of AMOS (Ji et al., 2022) because of computational constraints, and only selected the frontal views from CheXpert (Irvin et al., 2019).

Moreover, some of the datasets used do not have a predefined test set. On these datasets, we used systemic sampling to divide the dataset into train, evaluation, and test subsets. All the datasets used are publicly available, and we provide a link for downloading our specific train, validation, and test split in Section 6. Moreover, The data pre-processing pipeline is also available in the GitHub repository in Section 6.

The datasets were chosen based on the diversity of tasks and modalities and not on their clinical usefulness or value. Classifying different brain tumors types might not be a clinically applicable task, but we still included it in our analysis to gauge how each model performs in disease classification with MRI examinations.

3.3 Evaluation Settings

In our analysis, we focused mainly on the “out-of-the-box" performance of DINOv2, where we trained classification or segmentation heads while keeping the backbone frozen. This resulted in preferable lightweight training that requires fewer labeled instances, computational resources, and training time. Additionally, we also performed end-to-end fine-tuning and parameter-efficient fine-tuning evaluations for performance comparison to this lightweight training paradigm.

Table 1: The datasets used. For datasets that do not have a standardized test set, we chose the test set using systematic sampling. All the datasets and splits are public.

Dataset	Exam.	Task	Labels	# Classes	# Images/Volumes	Dim
NIH Chest X-ray (Wang et al., 2017)	X-ray	CLS	Thorax Diseases	14	112,120	2D
CheXpert (Irvin et al., 2019)	X-ray	CLS	Thorax Diseases	5	161,792	2D
Montgomery County (MC) (Jaeger et al., 2014)	X-ray	SEG	Lung	3	138	2D
SARS-CoV-2 (Soares et al., 2020)	CT	CLS	COVID-19 Diagnosis	2	210	3D
AMOS (Ji et al., 2022)	CT	SEG	Abdominal Organs	15	150	3D
MSD Spleen (Antonelli et al., 2022)	CT	SEG	Spleen	2	40	3D
MSD Hipp (Antonelli et al., 2022)	MRI	SEG	Hippocampus Head and Body	3	260	3D
MSD Heart (Antonelli et al., 2022)	MRI	SEG	Left Atrium	2	20	3D
Brain Tumor (Cheng et al., 2015)	MRI	CLS	Tumor Types	3	3,064	2D

We experimented with the original DINOv2 ViT-g/14 and the three smaller distilled versions (ViT-L/14, ViT-B/14, and ViT-S/14). We compared the performance and generalizability of DINOv2 to supervised, self-supervised, and weakly-supervised models. Table 2 detailed all the models used.

Table 2: Models used. Description of the backbones used along with their parameter count and pre-training settings. "Used For" describes what we used each model for and "# Images" describes the number of images in the pre-training dataset.

Method	Architecture	Dataset	Used For	# Images	# Params.	Citation
			Supervised			
CLS	DenseNet201	ImageNet1k	CLS	1.3M	20M	(Huang et al., 2018)
	ResNet152	ImageNet1k	CLS	1.3M	60M	(He et al., 2016)
	VGG19	ImageNet1k	CLS	1.3M	144M	(Simonyan & Zisserman, 2015)
	ViT-L/16	ImageNet21k	CLS, SEG	14M	300M	(Dosovitskiy et al., 2021)
SAM	ViT-L/16	SA-1B	CLS, SEG	11M	300M	(Kirillov et al., 2023)
			Weakly-Supervised			
CLIP	ViT-L/14	WIT-400M	CLS, SEG	400M	300M	(Radford et al., 2021)
OpenCLIP	ViT-H/14	LAION-2B	CLS, SEG	2,000M	632M	(Ilharco et al., 2021)
			Self-Supervised			
MAE	ViT-L/16	ImageNet1k	CLS, SEG	1.3M	300M	(He et al., 2021)
MSN	ViT-L/16	ImageNet1k	CLS, SEG	1.3M	300M	(Assran et al., 2022)
DINOv2	ViT-S/14	LVD-142M	CLS	142M	21M	(Oquab et al., 2023)
	ViT-B/14	LVD-142M	CLS	142M	86M	(Oquab et al., 2023)
	ViT-L/14	LVD-142M	CLS, SEG	142M	300M	(Oquab et al., 2023)
	ViT-g/14	LVD-142M	CLS, SEG	142M	1,100M	(Oquab et al., 2023)

A critical part of our work is that we standardized the training and hyperparameter tuning pipeline for each model and evaluation task, with the goal of isolating model performance. In this way, we can gain a clearer understanding of which models perform best under the same evaluation settings.

Disease Classification. We performed four main types of experiments: kNN, linear-probing, few-shot learning, and fine-tuning. (1) kNN was performed on the normalized features of the last backbone layer. (2) For linear-probing, a single linear layer was attached on top of the backbone. (3) In few-shot learning, we trained a linear layer on top of frozen features. (4) For fine-tuning, we used both parameter-efficient fine-tuning methods like LoRA (Hu et al., 2021) and BitFit (Zaken et al., 2022) and end-to-end fine-tuning.

When performing linear-probing with ViT architectures (Dosovitskiy et al., 2021), the linear layer takes either the CLS token or the CLS token concatenated with the average of all patch tokens, depending on which method yielded higher performance in the validation set. In multi-labeled classification, we predicted each class as a binary and averaged the model's result across all classes, and we used the method described by (Zhang & Zhou, 2007) for kNN. For 3D volumes, the embeddings for all slices were averaged before being passed into the classification head.

Organ Segmentation. For organ segmentation evaluations, we kept the encoder frozen and attached a U-Net, hierarchical decoder on top. The U-Net decoder is made up of four blocks, where each block consists of one convolutional layer along with ReLU activation function and batch normalization. Skip connections were obtained from the previous four blocks of the transformer model and concatenated to the features at each U-Net layer, as is done in the classical U-Net architecture (Ronneberger et al., 2015).

We also compared the performance of DINOv2 to segmentation architectures that are commonly used in medical image analysis including U-Net and TransUnet, trained end-to-end in a supervised fashion, and experimented with using a lightweight single linear layer decoder as a comparison with the U-Net decoder. For processing 3D volumes, we segmented each slice independently.

Comparison with medical-image pre-trained models. It is important to note that we do not compare DINOv2 to domain specific models like MedCLIP (Wang et al., 2022), BiomedCLIP Zhang et al. (2024), MedSAM (Ma et al., 2023), or other medical image pre-trained models. The goal of this work is evaluate whether DINOv2 pre-trained models can learn general-purpose representations in the medical domain that are useful across medical image analysis tasks like disease classification and organ segmentation, and across different radiology modalities like X-ray, CT, and MRI. All models used are pre-trained on natural images.

4 Results

In this section, we report our results across the different evaluation settings, tasks, and radiological modalities. We compare the performance of DINOv2 to weakly-supervised models including CLIP (Radford et al., 2021) and OpenCLIP (Ilharco et al., 2021), and self-supervised models including MAE (He et al., 2021) and MSN (Assran et al., 2022), and supervised models. We used the area under the operating receiver curve (AUROC) as a performance metric for classification tasks, and the average of the dice and jaccard scores as a metric for segmentation. We report only the best checkpoint across the epochs tested for each model.

In Section 4.1 and we will evaluate DINOv2 on disease classification and organ segmentation tasks. For segmentation, we will also show a comparison between using a linear layer decoder and a U-Net, hierarchical decoder on top of the frozen DINOv2 ViT-L/14 features. After that, in Section 4.2, we will analyze the cross-task generalizability of DINOv2 compared to the other models on disease classification and organ segmentation tasks. Then, in Section 4.3, we will explore the few-shot learning capability of DINOv2 on both disease classification and organ segmentation tasks. In Section 4.4, we perform parameter-efficient fine-tuning to compare the performance and efficiency of using PEFT with end-to-end fine-tuning and linear probing. Finally, 4.5 shows qualitative results of DINOv2 features on X-ray, CT, MRI modalities, and organ segmentation results of linear and U-Net decoders trained on top of frozen DINOv2 ViT-L/14 features.

4.1 Disease Classification and Organ Segmentation

We will start by analyzing the performance of DINOv2 ViT-g/14 and ViT-L/14 on linear-probing. Figure 3 shows the AUROC scores of both DINOv2 models compared to weakly-supervised and self-supervised models on four disease classification benchmarks. DINOv2 outperforms all other models on the more difficult large X-ray datasets and achieves performance closer to weakly-supervised models that are trained on much larger datasets. The ViT-L version of the model seemingly underperforms on 3D CT classification but is competitive with the ViT-g/14 version on all other classification tasks. Additionally Table 3 shows the linear-probing performance of all DINOv2 models compared to supervised learning methods on X-ray, CT, and MRI disease classification datasets. DINOv2 performs on

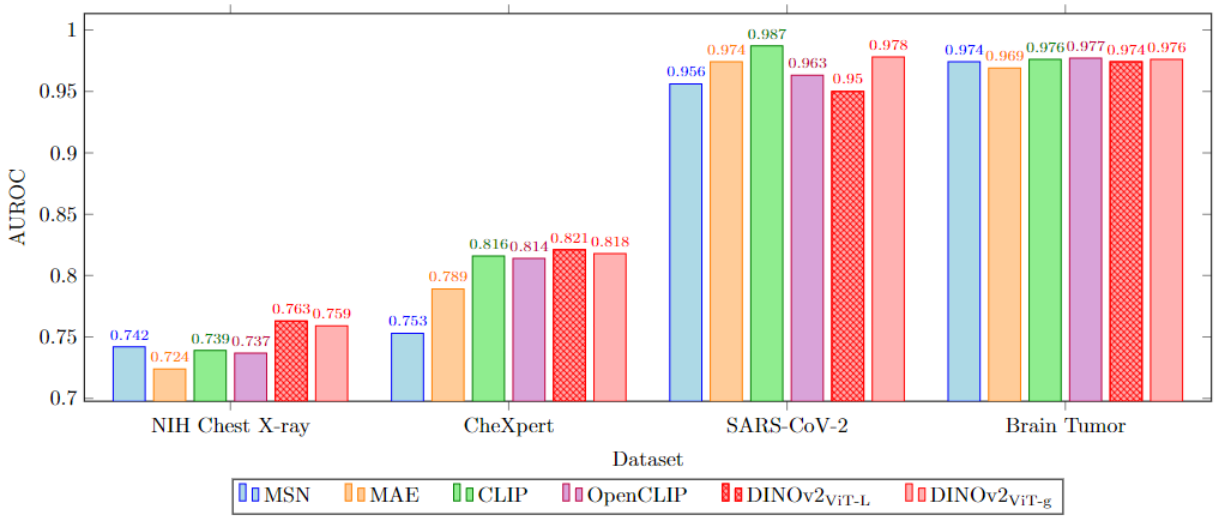

Figure 3: Linear probing for disease classification compared to self-supervised and weakly-supervised methods. The figure shows the performance of linear probing DINOv2 compared to other self-supervised and weakly-supervised models.

par or slightly better compared to supervised methods, and outperforms by a relatively larger margin commonly-used CNN supervised models.

Table 3: Linear probing for disease classification compared to supervised methods. The Table compares supervised models with DINOv2 pre-trained models in Linear-probing settings on X-ray, CT, and MRI datasets. All models were tested under the same settings.

Method	Architecture	NIH Chest X-ray	CheXpert	SARS-CoV-2	Brain Tumor
Supervised	DenseNet201	0.735	0.795	0.973	0.960
	ResNet152	0.718	0.779	0.936	0.948
	VGG19	0.696	0.750	0.891	0.933
	ViT-L/16	0.751	**0.829**	**0.983**	<u>0.975</u>
DINOv2	ViT-S/14	0.747	0.805	0.943	0.962
	ViT-B/14	0.755	0.812	0.922	0.972
	ViT-L/14	**0.763**	<u>0.821</u>	0.950	0.974
	ViT-g/14	<u>0.759</u>	0.818	<u>0.978</u>	**0.976**

Table 4 shows the kNN, linear-probing, and end-to-end fine-tuning results of DINOv2 compared to other supervised, weakly-supervised, and self-supervised methods on the NIH Chest X-ray and CheXpert datasets. Just like in linear probing, DINOv2 outperforms self-supervised methods in end-to-end fine-tuning but is competitive with weakly-supervised and supervised methods. Also important to highlight that DINOv2 under-performs on kNN evaluations compared to other methods, even though its features were designed to maximize kNN results. This might be explained by the domain shift between natural images in the pre-training and medical images, making the out-of-the-box kNN evaluations more random.

Moreover, we provide a comparison for segmentation tasks in Table 5. When comparing just image sizes of 224x224, DINOv2 performs the second-best, just behind MAE, which outperforms DINOv2 on all but one segmentation task. This can be explained given MAE's inherently pixel-level learning objective. An important point to note here is that all models except DINOv2 were pre-trained on image sizes of 224x224. At the end of the DINOv2 pre-training, it was adapted to image size 518x518, leading to worse performance on smaller

Table 4: DINOv2 performance comparison on large X-ray datasets. DINOv2 outperforms other methods on Linear-probing and fine-tuning but under performs on kNN evaluations. Multiple learning rates for tuning each backbones were tested, and only the best is shown.

		NIH Chest X-ray			CheXpert		
Method	Architecture	kNN	Linear-probing	Fine-tuning	kNN	Linear-probing	Fine-tuning
Supervised	DenseNet201	**0.675**	0.735	0.769	0.783	0.795	**0.882**
	Resnet152	0.668	0.718	0.752	0.766	0.779	0.868
	VGG19	0.644	0.696	0.711	0.728	0.750	0.870
	ViT-L/16	0.663	0.751	0.761	0.777	**0.829**	0.873
MAE	ViT-L/16	0.659	0.724	0.743	0.785	0.789	0.821
MSN	ViT-L/16	0.692	0.742	0.707	**0.807**	0.753	0.802
CLIP	ViT-L/14	0.655	0.739	0.697	0.742	0.816	0.842
OpenCLIP	ViT-H/14	0.659	0.737	**0.770**	0.744	0.814	0.847
DINOv2	ViT-L/14	0.663	**0.763**	0.717	0.771	0.821	0.786
	ViT-g/14	0.659	0.759	0.769	0.768	0.818	0.848

Table 5: DINOv2 on organ segmentation. A comparison between using a frozen DINOv2 backbone and other commonly-used segmentation models initialized from scratch.

Method	Architecture	MC	AMOS	MSD Heart	MSD Hipp	MSD Spleen
MAE	ViT-L/16	0.969	0.547	0.864	0.799	0.853
MSN	ViT-L/16	0.961	0.407	0.810	0.788	0.784
CLIP	ViT-L/14	0.955	0.445	0.762	0.748	0.747
OpenCLIP	ViT-H/14	0.962	0.501	0.793	0.779	0.803
DINOv2	ViT-L/14_{224}	0.966	0.512	0.792	**0.812**	0.813
	ViT-L/14_{448}	**0.974**	0.592	0.869	0.789	0.898
	ViT-g/14_{224}	0.966	0.511	0.804	0.761	0.802
	ViT-g/14_{448}	0.973	**0.642**	**0.875**	0.729	**0.900**

image sizes due to positional encoding interpolation (Oquab et al., 2023). Even then, DINOv2 still outperforms weakly-supervised models and MSN pre-training. When using image sizes closer to DINOv2's pre-training, it outperforms all other methods. However, it is difficult to determine how much of this increased performance is due to reduced interpolation of positional encoding or to higher details resulting from the larger images.

Table 6: DINOv2 compared to segmentation architectures. A comparison between using a frozen DINOv2 backbone and other commonly-used segmentation models initialized from scratch. The parameter count given is when there is one output class.

Method	Architecture	Trainable Params.	Total Params.	MC	AMOS	MSD Heart	MSD Hipp	MSD Spleen
Scratch	U-Net	31M (100%)	31M	0.973	0.432	**0.911**	0.593	0.826
	TransUnet	324M (100%)	324M	**0.974**	0.535	0.892	**0.821**	0.855
DINOv2	ViT-L/14	17M (5%)	317M	**0.974**	0.592	0.869	0.789	0.898
	ViT-g/14	38M (3%)	1,138M	0.973	**0.642**	0.875	0.729	**0.900**

DINOv2 compared to segmentation architectures. In Table 6 we compare U-Net decoders on top of frozen DINOv2 ViT-L/14 and ViT-g/14 features with U-Net and TransUnet models trained end-to-end from scratch. The results of all models are similar on the easier MC dataset, but DINOv2 outperforms the other U-Net and TransUnet on the more difficult AMOS multi-organ segmentation task even with a frozen encoder and less trainable parameters. On the MSD datasets, DINOv2 is competitive but there is variability in the performance.

U-Net vs linear decoders. Table 4 shows a performance comparison between using a linear layer decoder and a U-Net decoder on top of frozen DINOv2 ViT-L/14 features on the organ segmentation datasets. The linear layer decoder evaluations are used to isolate the performance of the DINOv2 encoder, analogous to the purpose of kNN classification evaluations. On the MC dataset where the target mask is large, linear and U-Net performance is comparable, highlighting the strong out-of-the-box features of DINOv2. The gap in performance increases, however, on MSD datasets where target masks are usually much smaller, making them harder to predict with a single layer. Figure 6 shows qualitative segmentation for both methods.

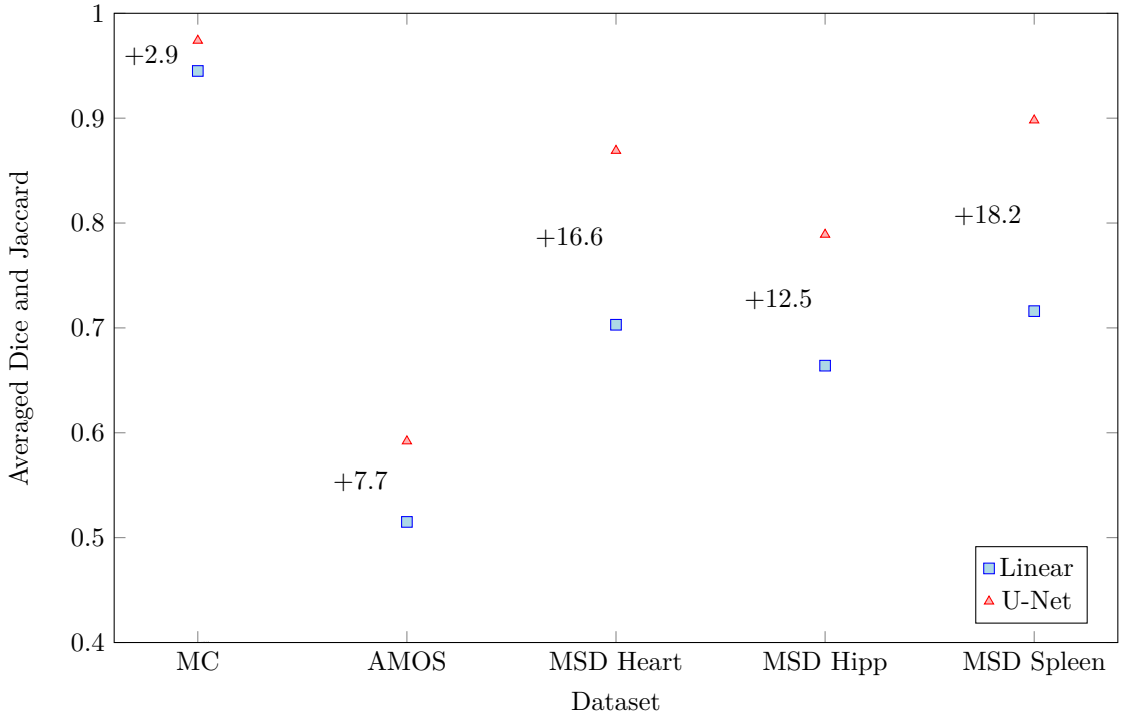

Figure 4: Linear vs. U-Net decoder. Comparison of the Linear and U-Net decoders on the four segmentation tasks used in this analysis. The backbones used in both is a DINOv2 ViT-L/14.

4.2 Cross-task Generalizability Analysis

In this section, we evaluate whether DINOv2 can produce representations that are more generalizable across tasks, compared to other models. To accomplish this task, we plot in Figure 1 the relative performance of weakly-supervised and self-supervised methods across disease classification and organ segmentation. The horizontal axis shows the relative performance or ranking of each of the models on segmentation tasks, while the vertical axis does the same for classification tasks. The ranking is calculated as the average ranking across all segmentation or classification tasks, where rank 1 means the model performs the best relative to the other models. Specifically, we assigned a score between 1 to 6 for each model on each dataset where a score of 6 means that the model achieved the highest result and 1 means the lowest. We averaged the scores for all datasets and plotted the ranking for each model based on this score, by assigning rank 1 to the highest score. An interesting observation is that models pre-trained with weakly-supervised learning perform well only on classification tasks, while MAE performs well only on segmentation. DINOv2 can generalize across both tasks and outperforms all other models for classification.

DINOv2 corss-task generalizability compared to supervised methods. Additionally, we carry out two experiments to compare the task-generalizability of DINOv2 with supervised methods. First, we compare the segmentation performance of a DINOv2 pre-trained ViT-L/14 with a ViT-L/16 pre-trained with supervised learning on ImageNet21k. Table 7 shows the results. DINOv2 outperforms the supervised ViT on 4 out of the 5 organ segmentation tasks, especially in the challenging AMOS multi-organ segmentation task.

Our second experiment compares the performance of the SAM image encoder with DINOv2 on classification tasks. SAM was trained for prompt-based segmentation and does not have a CLS token. To perform classification with SAM we averaged all the patch embeddings and treated the result as a CLS token. Table 8 shows the results. Images are of size 1024x1024 and only a subset of each dataset was used because of computational limits. DINOv2 significantly outperforms SAM on both datasets, highlighting the cross-task generalizability of the model.

Table 7: DINOv2 vs. ImageNet21k pre-trained ViT on organ segmentation. DINOv2 outperforms the supervised pre-trained ViT on 4 of the 5 tasks.

Method	Architecture	Image Size	Montgomery County	AMOS	MSD Heart	MSD Hipp	MSD Spleen
Supervised	ViT-L/16	224	0.963	0.433	0.825	0.750	0.773
DINOv2	ViT-L/14	224	0.966	0.512	0.792	0.812	0.813
	ViT-L/14	448	0.974	0.592	0.869	0.789	0.898

Table 8: SAM vs DINOv2 on X-ray on disease classification. Only a subset of the entire dataset was and all the images are of size 1024x1024. The average of patch embeddings were used as a CLS token for SAM.

Method	Architecture	NIH Chest X-ray	CheXpert
SAM	ViT-L/16	0.714	0.792
DINOv2	ViT-L/14	**0.755**	**0.816**

4.3 Few-shot Learning

To measure DINOv2's ability to adapt to new distributions using a few labeled instances, we perform few-shot learning for both disease classification and organ segmentation on X-ray datasets.

At the top row of Figure 5, we start by comparing DINOv2 ViT-L/14 to weakly-supervised and self-supervised methods. The top-left subplot shows the performance on the NIH Chest X-ray disease classification dataset, while the top-right subplot shows the performance on the MC lung segmentation datasets. For disease classification, there is no clear trend when the number of patients used for each class is between 1 and 4, but when 8 patients are used, DINOv2 outperforms all other methods. For organ segmentation, DINOv2 outperforms all other methods from the start and is only worse than MAE when the entire dataset is used.

A similar trend can be observed at the bottom row of Figure 5, where we compare DINOv2 with supervised methods. The bottom-left subplot shows that DINOv2 outperforms other methods when the number of patients are 8 or more, but to a lesser degree compared to self-supervised and weakly-supervised methods. For organ segmentation, DINOv2 outperforms other models by a large margin when using less than eight instances, which is somewhat expected given it was pre-trained while the other segmentation models were not.

4.4 Parameter-efficient Fine-tuning

We experiment with parameter-efficient fine-tuning (PEFT) techniques on DINOv2 ViT-g/14, which, as a whole, contains 1.1 billion parameters. PEFT methods are used to enable efficient adaptation of large models to downstream tasks, usually achieving performance

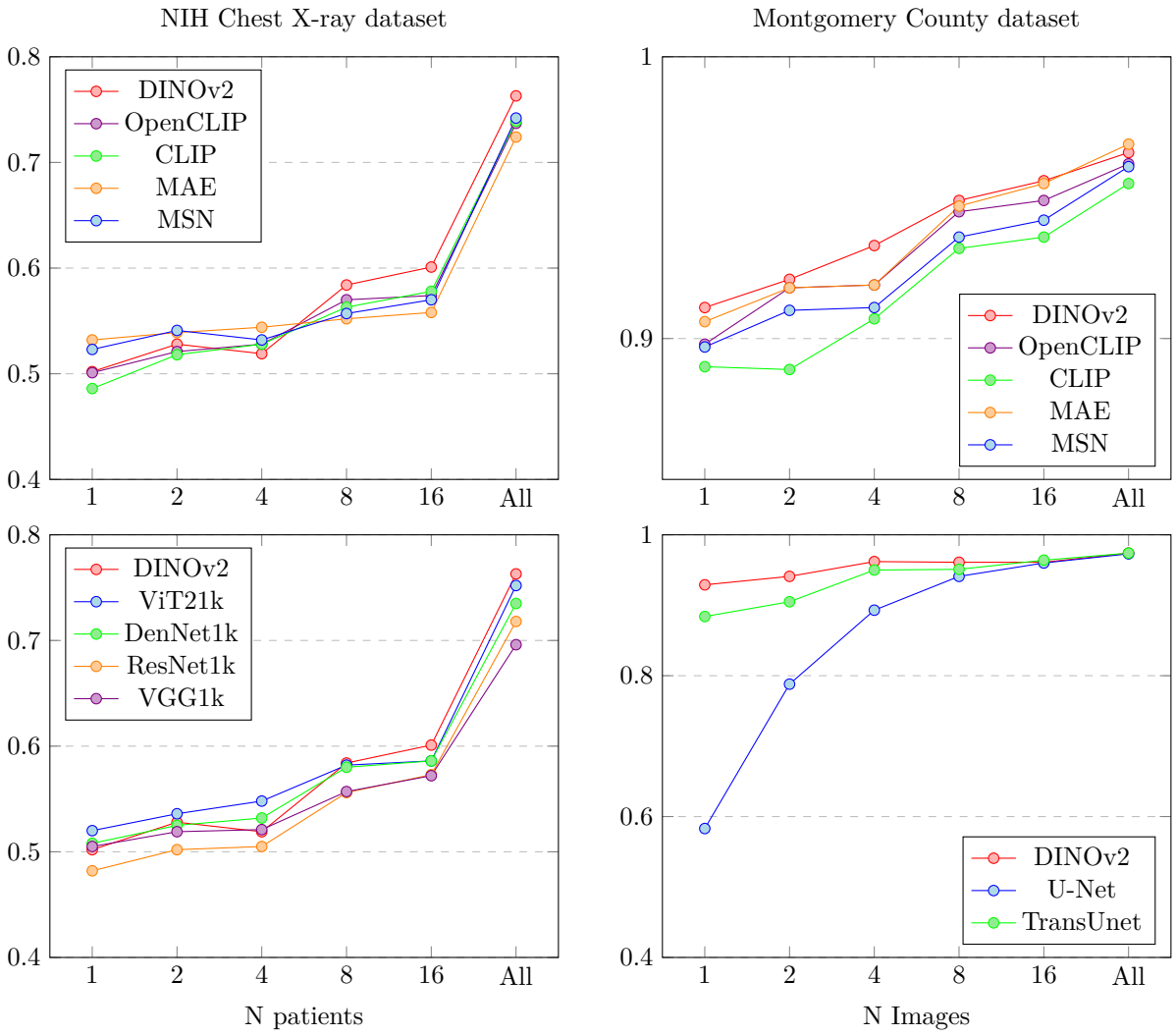

Figure 5: Few-shot disease classification and organ segmentation. The top row compares DINOv2 ViT-L/14 with weakly-supervised and self-supervised methods on the NIH Chest X-ray and MC datasets. The bottom row provides a comparison with supervised methods. For disease classification, there is no clear trend when the number of patients used for each class is between 1 and 4, but when 8 patients are used, DINOv2 clearly outperforms all other methods. For organ segmentation DINOv2 outperforms all other methods from the start.

that is on par with end-to-end fine-tuning while requiring a lot less compute and memory. Previous work by Dutt et al. (2023) has highlighted the opportunity of employing PEFT to tune large foundation models for medical image analysis.

We employ two different PEFT techniques: LoRA (Hu et al., 2021) and BitFit (Zaken et al., 2022). LoRA is an additive method that inserts trainable decomposition matrices in the layers of a transformer, while BitFit is a selective method that unfreezes only the bias terms of the model. Table 9 shows a result and efficiency comparison between the two PEFT methods with a comparison to end-to-end fine-tuning and linear-probing on the NIH Chest X-ray and CheXpert datasets using the DINOv2 ViT-g/14 model.

Table 9: PEFT on DINOv2 ViT-g/14. Both LoRA and BitFit achieve results that are better than linear-probing while adapting less than 1% of the total parameters.

Method	Trainable Params. (%)	NIH Chest X-ray	CheXpert
Fine-tuning	1,100M (100%)	0.769	0.848
Linear-probing	1,500 (1e-6%)	0.759	0.818
LoRA	8M (0.7%)	0.767	0.823
BitFit	0.8M (0.07%)	0.768	0.817

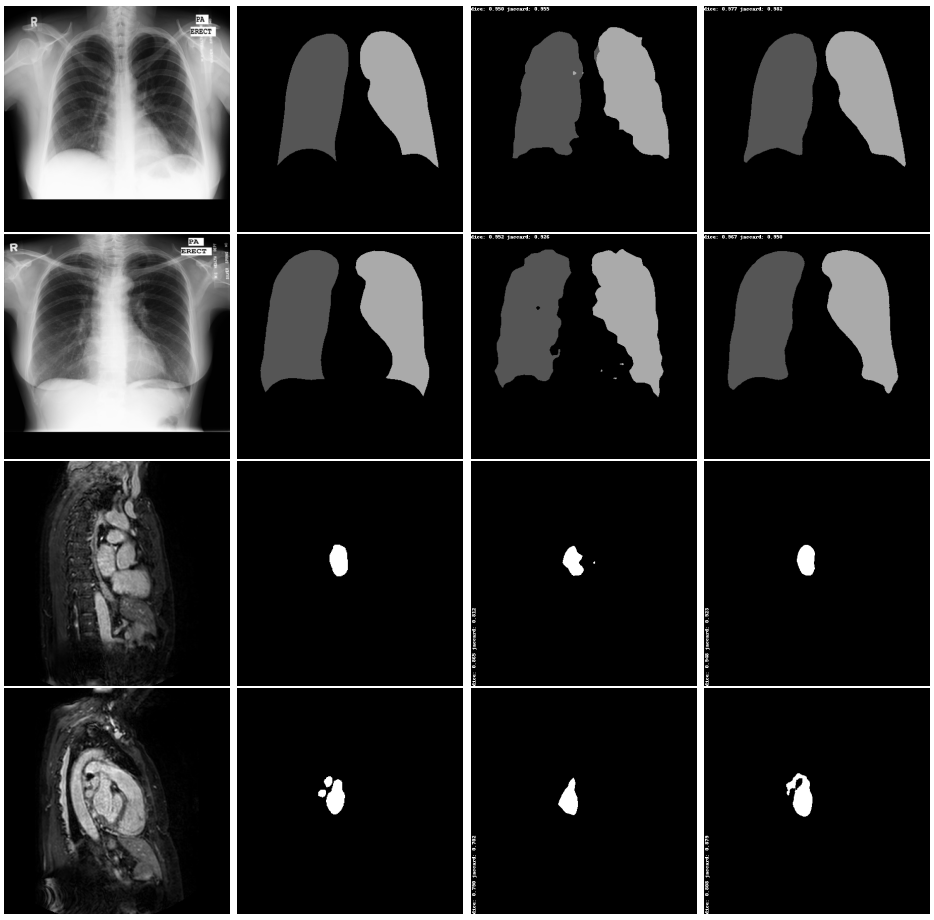

Figure 6: Linear vs. U-Net visualization. The figure shows a qualitative comparison between segmentation masks generated by the linear layer and the U-Net decoder.

4.5 Qualitative Results

In this section we will show qualitative results of DINOv2 features using principal component analysis (PCA) performed on DINOv2 patch features on X-ray, CT, and MRI scans, following the method delineated in (Oquab et al., 2023). We will also provide organ segmentation results of linear compared U-Net decoders.

PCA visualization. Figure 2 shows the first three PCA components. The PCA is computed between patches of images that are in the same column, and the first 3 components are shown for X-ray, CT, and MRI scans. Thresholding is used on the first PCA component to remove the background. Just like in natural images (Oquab et al., 2023), the colors of the three PCA components correspond well with the same parts of images in the same category. This is an easier task however, compared to natural images, because there is less variability between examinations on medical images compared to natural images.

U-Net and linear decoder visualization. We also show a visualization of linear and U-Net decoders trained on top of DINOv2 ViT-L/14 features. The linear layer decoder performs surprisingly well, but is limited, especially on smaller masks, due to the smaller decoding map (32x32 pixels interpolated to 448x448) and less adjustable parameters. As expected, the U-Net segmentation results are smoother and represents the ground truth mask more accurately, but is still limited due to the frozen encoder.

5 Discussion

Foundation models have shown promise for reducing the data annotation problem and increasing model generalizability and robustness. Thus they are a direction towards increasing performance and adoption of deep learning systems in healthcare. However, training a foundation model from scratch is extremely challenging for most institutions, demanding substantial amounts of well-organized data and computational resources. This challenge is particularly pronounced in the realm of medical image analysis, where data annotation is markedly more expensive than in other fields, and the data itself comprises high-dimensional volumes. This paper examines DINOv2, a foundation model trained on natural images, for medical applications. The DINOv2 pre-training approach is specifically promising given its ability to learn general-purpose representations and perform well out-of-the-box, without needing to fine-tune the encoder. We believe that using DINOv2 pre-training on medical data is a promising approach for future research aimed at building large-scale medical foundation models without supervision.

6 Conclusion

In this work, we examine DINOv2, a self-supervised foundation model pre-trained on 142 million natural images, for applications to radiology image analysis across X-ray, CT, and MRI modalities. We conclude that DINOv2 is a strong feature extractor across both disease classification and organ segmentation tasks, and outperforms traditional ImageNet pre-trained CNN methods and other weakly-supervised and self-supervised pre-trained ViTs.

Reproducibility

All of the data used for this work is publicly available, and our train, validation, and test split are available here. All the training and validation logs, hyper-parameters, and model weights are available here.

References

Michela Antonelli, Annika Reinke, Spyridon Bakas, Keyvan Farahani, Annette Kopp-Schneider, Bennett A. Landman, Geert Litjens, Bjoern Menze, Olaf Ronneberger,

Ronald M. Summers, Bram van Ginneken, Michel Bilello, Patrick Bilic, Patrick F. Christ, Richard K. G. Do, Marc J. Gollub, Stephan H. Heckers, Henkjan Huisman, William R. Jarnagin, Maureen K. McHugo, Sandy Napel, Jennifer S. Golia Pernicka, Kawal Rhode, Catalina Tobon-Gomez, Eugene Vorontsov, James A. Meakin, Sebastien Ourselin, Manuel Wiesenfarth, Pablo Arbeláez, Byeonguk Bae, Sihong Chen, Laura Daza, Jianjiang Feng, Baochun He, Fabian Isensee, Yuanfeng Ji, Fucang Jia, Ildoo Kim, Klaus Maier-Hein, Dorit Merhof, Akshay Pai, Beomhee Park, Mathias Perslev, Ramin Rezaiifar, Oliver Rippel, Ignacio Sarasua, Wei Shen, Jaemin Son, Christian Wachinger, Liansheng Wang, Yan Wang, Yingda Xia, Daguang Xu, Zhanwei Xu, Yefeng Zheng, Amber L. Simpson, Lena Maier-Hein, and M. Jorge Cardoso. The medical segmentation decathlon. *Nature Communications*, 13(1), jul 2022. doi: 10.1038/s41467-022-30695-9. URL `https://doi.org/10.1038%2Fs41467-022-30695-9`.

Mahmoud Assran, Mathilde Caron, Ishan Misra, Piotr Bojanowski, Florian Bordes, Pascal Vincent, Armand Joulin, Michael Rabbat, and Nicolas Ballas. Masked siamese networks for label-efficient learning, 2022.

Josue Ortega Caro, Antonio H. de O. Fonseca, Christopher Averill, Syed A. Rizvi, Matteo Rosati, James L. Cross, Prateek Mittal, Emanuele Zappala, Daniel Levine, Rahul M. Dhodapkar, Chadi G. Abdallah, and David van Dijk. Brainlm: A foundation model for brain activity recordings. *bioRxiv*, 2023. doi: 10.1101/2023.09.12.557460. URL `https://www.biorxiv.org/content/early/2023/09/13/2023.09.12.557460`.

Mathilde Caron, Hugo Touvron, Ishan Misra, Hervé Jégou, Julien Mairal, Piotr Bojanowski, and Armand Joulin. Emerging properties in self-supervised vision transformers, 2021.

Pierre Chambon, Christian Bluethgen, Jean-Benoit Delbrouck, Rogier Van der Sluijs, Małgorzata Połacin, Juan Manuel Zambrano Chaves, Tanishq Mathew Abraham, Shivanshu Purohit, Curtis P. Langlotz, and Akshay Chaudhari. Roentgen: Vision-language foundation model for chest x-ray generation, 2022a.

Pierre Chambon, Christian Bluethgen, Curtis P. Langlotz, and Akshay Chaudhari. Adapting pretrained vision-language foundational models to medical imaging domains, 2022b.

Jun Cheng, Wei Huang, Shuangliang Cao, Ru Yang, Wei Yang, Zhaoqiang Yun, Zhijian Wang, and Qianjin Feng. Enhanced performance of brain tumor classification via tumor region augmentation and partition. *PLOS ONE*, 10(10):1–13, 10 2015. doi: 10.1371/journal.pone.0140381. URL `https://doi.org/10.1371/journal.pone.0140381`.

Joseph Paul Cohen, Mohammad Hashir, Rupert Brooks, and Hadrien Bertrand. On the limits of cross-domain generalization in automated x-ray prediction. In Tal Arbel, Ismail Ben Ayed, Marleen de Bruijne, Maxime Descoteaux, Herve Lombaert, and Christopher Pal (eds.), *Proceedings of the Third Conference on Medical Imaging with Deep Learning*, volume 121 of *Proceedings of Machine Learning Research*, pp. 136–155. PMLR, 06–08 Jul 2020. URL `https://proceedings.mlr.press/v121/cohen20a.html`.

Jia Deng, Wei Dong, Richard Socher, Li-Jia Li, Kai Li, and Li Fei-Fei. Imagenet: A large-scale hierarchical image database. In *2009 IEEE Conference on Computer Vision and Pattern Recognition*, pp. 248–255, 2009. doi: 10.1109/CVPR.2009.5206848.

Alexey Dosovitskiy, Lucas Beyer, Alexander Kolesnikov, Dirk Weissenborn, Xiaohua Zhai, Thomas Unterthiner, Mostafa Dehghani, Matthias Minderer, Georg Heigold, Sylvain Gelly, Jakob Uszkoreit, and Neil Houlsby. An image is worth 16x16 words: Transformers for image recognition at scale, 2021.

Raman Dutt, Linus Ericsson, Pedro Sanchez, Sotirios A. Tsaftaris, and Timothy Hospedales. Parameter-efficient fine-tuning for medical image analysis: The missed opportunity, 2023.

Li Fei-Fei, R. Fergus, and P. Perona. Learning generative visual models from few training examples: An incremental bayesian approach tested on 101 object categories. In *2004 Conference on Computer Vision and Pattern Recognition Workshop*, pp. 178–178, 2004. doi: 10.1109/CVPR.2004.383.

Ali Hatamizadeh, Vishwesh Nath, Yucheng Tang, Dong Yang, Holger Roth, and Daguang Xu. Swin unetr: Swin transformers for semantic segmentation of brain tumors in mri images. *arXiv preprint arXiv:2201.01266*, 2022.

Kaiming He, Xiangyu Zhang, Shaoqing Ren, and Jian Sun. Deep residual learning for image recognition. In *2016 IEEE Conference on Computer Vision and Pattern Recognition (CVPR)*, pp. 770–778, 2016. doi: 10.1109/CVPR.2016.90.

Kaiming He, Xinlei Chen, Saining Xie, Yanghao Li, Piotr Dollár, and Ross Girshick. Masked autoencoders are scalable vision learners, 2021.

Sheng He, Rina Bao, Jingpeng Li, Jeffrey Stout, Atle Bjornerud, P. Ellen Grant, and Yangming Ou. Computer-vision benchmark segment-anything model (sam) in medical images: Accuracy in 12 datasets, 2023.

Edward J. Hu, Yelong Shen, Phillip Wallis, Zeyuan Allen-Zhu, Yuanzhi Li, Shean Wang, Lu Wang, and Weizhu Chen. Lora: Low-rank adaptation of large language models, 2021.

Gao Huang, Zhuang Liu, Laurens van der Maaten, and Kilian Q. Weinberger. Densely connected convolutional networks, 2018.

Shah Hussain, Iqra Mubeen, Niamat Ullah, Syed Shahab Ud Din Shah, Bakhtawar Abduljalil Khan, Muhammad Zahoor, Riaz Ullah, Farhat Ali Khan, and Mujeeb A Sultan. Modern diagnostic imaging technique applications and risk factors in the medical field: A review. *Biomed Res. Int.*, 2022:1–19, June 2022.

Gabriel Ilharco, Mitchell Wortsman, Ross Wightman, Cade Gordon, Nicholas Carlini, Rohan Taori, Achal Dave, Vaishaal Shankar, Hongseok Namkoong, John Miller, Hannaneh Hajishirzi, Ali Farhadi, and Ludwig Schmidt. Openclip, July 2021. URL `https://doi.org/10.5281/zenodo.5143773`.

Jeremy Irvin, Pranav Rajpurkar, Michael Ko, Yifan Yu, Silviana Ciurea-Ilcus, Christopher Chute, Henrik Marklund, Behzad Haghgoo, Robyn L. Ball, Katie S. Shpanskaya, Jayne Seekins, David A. Mong, Safwan S. Halabi, Jesse K. Sandberg, Ricky Jones, David B. Larson, Curtis P. Langlotz, Bhavik N. Patel, Matthew P. Lungren, and Andrew Y. Ng. Chexpert: A large chest radiograph dataset with uncertainty labels and expert comparison. *CoRR*, abs/1901.07031, 2019. URL `http://arxiv.org/abs/1901.07031`.

Stefan Jaeger, Sema Candemir, Sameer Antani, Yì-Xiáng J Wáng, Pu-Xuan Lu, and George Thoma. Two public chest x-ray datasets for computer-aided screening of pulmonary diseases. *Quantitative imaging in medicine and surgery*, 4(6):475, 2014.

Yuanfeng Ji, Haotian Bai, Jie Yang, Chongjian Ge, Ye Zhu, Ruimao Zhang, Zhen Li, Lingyan Zhang, Wanling Ma, Xiang Wan, et al. Amos: A large-scale abdominal multi-organ benchmark for versatile medical image segmentation. *arXiv preprint arXiv:2206.08023*, 2022.

Alistair E W Johnson, Tom J Pollard, Seth J Berkowitz, Nathaniel R Greenbaum, Matthew P Lungren, Chih-Ying Deng, Roger G Mark, and Steven Horng. MIMIC-CXR, a de-identified publicly available database of chest radiographs with free-text reports. *Sci Data*, 6(1):317, December 2019.

Christopher J Kelly, Alan Karthikesalingam, Mustafa Suleyman, Greg Corrado, and Dominic King. Key challenges for delivering clinical impact with artificial intelligence. *BMC Medicine*, 17(1):195, October 2019.

Bangul Khan, Hajira Fatima, Ayatullah Qureshi, Sanjay Kumar, Abdul Hanan, Jawad Hussain, and Saad Abdullah. Drawbacks of artificial intelligence and their potential solutions in the healthcare sector. *Biomed Mater Devices*, pp. 1–8, February 2023.

Alexander Kirillov, Eric Mintun, Nikhila Ravi, Hanzi Mao, Chloe Rolland, Laura Gustafson, Tete Xiao, Spencer Whitehead, Alexander C. Berg, Wan-Yen Lo, Piotr Dollár, and Ross Girshick. Segment anything, 2023.

Bennett Landman, Zhoubing Xu, Juan Eugenio Igelsias, Martin Styner, Thomas Langerak, and Arno Klein. Miccai multi-atlas labeling beyond the cranial vault–workshop and challenge. In *International Workshop on Multimodal Brain Image Analysis*, pp. 1–10. Springer, 2015.

Jun Ma, Yuting He, Feifei Li, Lin Han, Chenyu You, and Bo Wang. Segment anything in medical images, 2023.

Maciej A. Mazurowski, Haoyu Dong, Hanxue Gu, Jichen Yang, Nicholas Konz, and Yixin Zhang. Segment anything model for medical image analysis: An experimental study. *Medical Image Analysis*, 89:102918, October 2023. ISSN 1361-8415. doi: 10.1016/j.media.2023.102918. URL `http://dx.doi.org/10.1016/j.media.2023.102918`.

Rick Merritt. What are foundation models? `https://blogs.nvidia.com/blog/what-are-foundation-models/`, March 2023. Accessed: 2023-11-30.

Michael Moor, Oishi Banerjee, Zahra Shakeri Hossein Abad, Harlan M. Krumholz, Jure Leskovec, Eric J. Topol, and Pranav Rajpurkar. Foundation models for generalist medical artificial intelligence. *Nature*, 616(7956):259–265, April 2023. ISSN 1476-4687. doi: 10.1038/s41586-023-05881-4. URL `http://dx.doi.org/10.1038/s41586-023-05881-4`.

Maxime Oquab, Timothée Darcet, Théo Moutakanni, Huy Vo, Marc Szafraniec, Vasil Khalidov, Pierre Fernandez, Daniel Haziza, Francisco Massa, Alaaeldin El-Nouby, Mahmoud Assran, Nicolas Ballas, Wojciech Galuba, Russell Howes, Po-Yao Huang, Shang-Wen Li, Ishan Misra, Michael Rabbat, Vasu Sharma, Gabriel Synnaeve, Hu Xu, Hervé Jegou, Julien Mairal, Patrick Labatut, Armand Joulin, and Piotr Bojanowski. Dinov2: Learning robust visual features without supervision, 2023.

Wei Peng, Li Feng, Guoying Zhao, and Fang Liu. Learning optimal k-space acquisition and reconstruction using physics-informed neural networks. In *Proceedings of the IEEE/CVF Conference on Computer Vision and Pattern Recognition*, pp. 20794–20803, 2022.

Jianing Qiu, Jian Wu, Hao Wei, Peilun Shi, Minqing Zhang, Yunyun Sun, Lin Li, Hanruo Liu, Hongyi Liu, Simeng Hou, Yuyang Zhao, Xuehui Shi, Junfang Xian, Xiaoxia Qu, Sirui Zhu, Lijie Pan, Xiaoniao Chen, Xiaojia Zhang, Shuai Jiang, Kebing Wang, Chenlong Yang, Mingqiang Chen, Sujie Fan, Jianhua Hu, Aiguo Lv, Hui Miao, Li Guo, Shujun Zhang, Cheng Pei, Xiaojuan Fan, Jianqin Lei, Ting Wei, Junguo Duan, Chun Liu, Xiaobo Xia, Siqi Xiong, Junhong Li, Benny Lo, Yih Chung Tham, Tien Yin Wong, Ningli Wang, and Wu Yuan. Visionfm: a multi-modal multi-task vision foundation model for generalist ophthalmic artificial intelligence, 2023.

Alec Radford, Jong Wook Kim, Chris Hallacy, Aditya Ramesh, Gabriel Goh, Sandhini Agarwal, Girish Sastry, Amanda Askell, Pamela Mishkin, Jack Clark, Gretchen Krueger, and Ilya Sutskever. Learning transferable visual models from natural language supervision, 2021.

Pranav Rajpurkar, Jeremy Irvin, Kaylie Zhu, Brandon Yang, Hershel Mehta, Tony Duan, Daisy Ding, Aarti Bagul, Curtis Langlotz, Katie Shpanskaya, Matthew P. Lungren, and Andrew Y. Ng. Chexnet: Radiologist-level pneumonia detection on chest x-rays with deep learning, 2017.

Olaf Ronneberger, Philipp Fischer, and Thomas Brox. U-net: Convolutional networks for biomedical image segmentation, 2015.

Karen Simonyan and Andrew Zisserman. Very deep convolutional networks for large-scale image recognition, 2015.

Eduardo Soares, Plamen Angelov, Sarah Biaso, Michele Higa Froes, and Daniel Kanda Abe. Sars-cov-2 ct-scan dataset: A large dataset of real patients ct scans for sars-cov-2 identification. *MedRxiv*, pp. 2020–04, 2020.

Yucheng Tang, Dong Yang, Wenqi Li, Holger R Roth, Bennett Landman, Daguang Xu, Vishwesh Nath, and Ali Hatamizadeh. Self-supervised pre-training of swin transformers for 3d medical image analysis. In *Proceedings of the IEEE/CVF Conference on Computer Vision and Pattern Recognition*, pp. 20730–20740, 2022.

Jeya Maria Jose Valanarasu, Yucheng Tang, Dong Yang, Ziyue Xu, Can Zhao, Wenqi Li, Vishal M. Patel, Bennett Landman, Daguang Xu, Yufan He, and Vishwesh Nath. Disruptive autoencoders: Leveraging low-level features for 3d medical image pre-training, 2023.

Xiaosong Wang, Yifan Peng, Le Lu, Zhiyong Lu, Mohammadhadi Bagheri, and Ronald M. Summers. Chestx-ray8: Hospital-scale chest x-ray database and benchmarks on weakly-supervised classification and localization of common thorax diseases. In *2017 IEEE Conference on Computer Vision and Pattern Recognition (CVPR)*, pp. 3462–3471, 2017. doi: 10.1109/CVPR.2017.369.

Zhao Wang, Chang Liu, Shaoting Zhang, and Qi Dou. Foundation model for endoscopy video analysis via large-scale self-supervised pre-train, 2023.

Zifeng Wang, Zhenbang Wu, Dinesh Agarwal, and Jimeng Sun. Medclip: Contrastive learning from unpaired medical images and text, 2022.

Tobias Weyand, Andre Araujo, Bingyi Cao, and Jack Sim. Google landmarks dataset v2 – a large-scale benchmark for instance-level recognition and retrieval, 2020.

Bin Xiao, Haiping Wu, Weijian Xu, Xiyang Dai, Houdong Hu, Yumao Lu, Michael Zeng, Ce Liu, and Lu Yuan. Florence-2: Advancing a unified representation for a variety of vision tasks, 2023.

Lu Yuan, Dongdong Chen, Yi-Ling Chen, Noel Codella, Xiyang Dai, Jianfeng Gao, Houdong Hu, Xuedong Huang, Boxin Li, Chunyuan Li, Ce Liu, Mengchen Liu, Zicheng Liu, Yumao Lu, Yu Shi, Lijuan Wang, Jianfeng Wang, Bin Xiao, Zhen Xiao, Jianwei Yang, Michael Zeng, Luowei Zhou, and Pengchuan Zhang. Florence: A new foundation model for computer vision, 2021.

Elad Ben Zaken, Shauli Ravfogel, and Yoav Goldberg. Bitfit: Simple parameter-efficient fine-tuning for transformer-based masked language-models, 2022.

Min-Ling Zhang and Zhi-Hua Zhou. Ml-knn: A lazy learning approach to multi-label learning. *Pattern recognition*, 40(7):2038–2048, 2007.

Sheng Zhang, Yanbo Xu, Naoto Usuyama, Hanwen Xu, Jaspreet Bagga, Robert Tinn, Sam Preston, Rajesh Rao, Mu Wei, Naveen Valluri, Cliff Wong, Andrea Tupini, Yu Wang,

Matt Mazzola, Swadheen Shukla, Lars Liden, Jianfeng Gao, Matthew P. Lungren, Tristan Naumann, Sheng Wang, and Hoifung Poon. Biomedclip: a multimodal biomedical foundation model pretrained from fifteen million scientific image-text pairs, 2024.

Yichi Zhang and Rushi Jiao. Towards segment anything model (sam) for medical image segmentation: A survey, 2023.

Yu Zhang, Wei Han, James Qin, Yongqiang Wang, Ankur Bapna, Zhehuai Chen, Nanxin Chen, Bo Li, Vera Axelrod, Gary Wang, Zhong Meng, Ke Hu, Andrew Rosenberg, Rohit Prabhavalkar, Daniel S. Park, Parisa Haghani, Jason Riesa, Ginger Perng, Hagen Soltau, Trevor Strohman, Bhuvana Ramabhadran, Tara Sainath, Pedro Moreno, Chung-Cheng Chiu, Johan Schalkwyk, Françoise Beaufays, and Yonghui Wu. Google usm: Scaling automatic speech recognition beyond 100 languages, 2023.

Yuhao Zhang, Hang Jiang, Yasuhide Miura, Christopher D. Manning, and Curtis P. Langlotz. Contrastive learning of medical visual representations from paired images and text, 2022.

Bolei Zhou, Hang Zhao, Xavier Puig, Sanja Fidler, Adela Barriuso, and Antonio Torralba. Scene parsing through ade20k dataset. In *2017 IEEE Conference on Computer Vision and Pattern Recognition (CVPR)*, pp. 5122–5130, 2017. doi: 10.1109/CVPR.2017.544.

Jinghao Zhou, Chen Wei, Huiyu Wang, Wei Shen, Cihang Xie, Alan Yuille, and Tao Kong. ibot: Image bert pre-training with online tokenizer, 2022.

Yukun Zhou, Mark A. Chia, Siegfried K. Wagner, Murat S. Ayhan, Dominic J. Williamson, Robbert R. Struyven, Timing Liu, Moucheng Xu, Mateo G. Lozano, Peter Woodward-Court, Yuka Kihara, Naomi Allen, John E. J. Gallacher, Thomas Littlejohns, Tariq Aslam, Paul Bishop, Graeme Black, Panagiotis Sergouniotis, Denize Atan, Andrew D. Dick, Cathy Williams, Sarah Barman, Jenny H. Barrett, Sarah Mackie, Tasanee Braithwaite, Roxana O. Carare, Sarah Ennis, Jane Gibson, Andrew J. Lotery, Jay Self, Usha Chakravarthy, Ruth E. Hogg, Euan Paterson, Jayne Woodside, Tunde Peto, Gareth Mckay, Bernadette Mcguinness, Paul J. Foster, Konstantinos Balaskas, Anthony P. Khawaja, Nikolas Pontikos, Jugnoo S. Rahi, Gerassimos Lascaratos, Praveen J. Patel, Michelle Chan, Sharon Y. L. Chua, Alexander Day, Parul Desai, Cathy Egan, Marcus Fruttiger, David F. Garway-Heath, Alison Hardcastle, Sir Peng T. Khaw, Tony Moore, Sobha Sivaprasad, Nicholas Strouthidis, Dhanes Thomas, Adnan Tufail, Ananth C. Viswanathan, Bal Dhillon, Tom Macgillivray, Cathie Sudlow, Veronique Vitart, Alexander Doney, Emanuele Trucco, Jeremy A. Guggeinheim, James E. Morgan, Chris J. Hammond, Katie Williams, Pirro Hysi, Simon P. Harding, Yalin Zheng, Robert Luben, Phil Luthert, Zihan Sun, Martin McKibbin, Eoin O'Sullivan, Richard Oram, Mike Weedon, Chris G. Owen, Alicja R. Rudnicka, Naveed Sattar, David Steel, Irene Stratton, Robyn Tapp, Max M. Yates, Axel Petzold, Savita Madhusudhan, Andre Altmann, Aaron Y. Lee, Eric J. Topol, Alastair K. Denniston, Daniel C. Alexander, and Pearse A. Keane. A foundation model for generalizable disease detection from retinal images. *Nature*, 622 (7981):156–163, September 2023. ISSN 1476-4687. doi: 10.1038/s41586-023-06555-x. URL `http://dx.doi.org/10.1038/s41586-023-06555-x`.